ADVANCED ENERGY MATERIALS
www.advenergymat.de

Reactive Inhibition Strategy for Triple-cation Mixed-halide Perovskite Ink with Prolonged Shelf-life

Zongcai Li, Zhi Xing, Haibin Peng, Xiangchuan Meng, Dengxue Li, Lu Huang, Xiaotian Hu, Ting Hu, and Yiwang Chen**

Solution processing of perovskite solar cells (PSCs) is highly promising for the high-throughput production of cost-effective devices. Although PSCs have achieved great advances in power conversion efficiency, challenges still remain in the reproducibility of high-quality perovskite thin film with simultaneously improved precursor solution stability. Here, a reactive inhibition strategy by introducing diethyl (hydroxymethyl) phosphonate (DHP) in perovskite precursor solution is successfully employed to improve the stability of precursor solution and the performance of corresponding device. DHP inhibits the reactivity of the iodide and formamidinium ions through multiple chemical bonds, ensuring the stability of the precursor solution. In addition, due to chelation interaction of Pb^{2+} with the oxygen of P=O in DHP, the DHP in the perovskite film improves the film quality with desired stoichiometry by reducing the defects and the content of lead iodide. The DHP-doped precursor solution and corresponding devices show excellent performance reproducibility and super stability under ambient conditions for more than 50 days, which illustrates the commercial feasibility for scalable fabrication.

1. Introduction

Owing to the excellent optoelectronic properties of organic-inorganic metal halide perovskite solar cells (PSCs), including solution-processability, controllable bandgap, and long charge carrier diffusion length, the PSCs have received increasing attention from researchers.[1–5] In past decade, the power conversion efficiency (PCE) of single-junction PSCs have risen from the initial 3.8% to 25.7%, which is high enough to be comparable to commercial silicon-based solar cells.[6,7] Moreover, solution processing can further shrink costs of PSCs, demonstrating its potential for commercial viability.[8] The high reproducibility of PSCs is crucial to their commercialization. Numerous strategies have been reported to improve the reproducibility of PSCs to date, such as two-step deposition,[9] hot casting method[10] and mix solvent approach,[11] and additive engineering.[12–19] However, the majority of these methods are based on fresh solutions for modification. Solution processing of PSCs is highly promising for the high-throughput production of cost-effective devices. Yet, stability of the precursor solution is rarely reported, and a precursor solution with high stability is the basis for obtaining highly reproducible PSCs. Solution-processed materials are chemically unstable under ambient conditions during solution aging, resulting in poor device reproducibility and bad performance.[20] Significantly, aging is more severe in the methylammonium (MA)/formamidinium (FA)/cesium (Cs) triple-cation mixed-halide perovskites due to the complex composition.

In order to enhance the stability of perovskite precursor solution, the aging mechanism of the precursor has been investigated. Firstly, MA will be generated by the deprotonation reaction of MA^+ due to the reversible acid-base decomposition, and the stoichiometric ratio of methylammonium iodide (MAI)/lead(II) iodide (PbI_2) changes finally in the precursor solution.[21,22] MA quickly condenses with highly active FA^+ of FAI to create N-methyl FAI (MFAI) and N, N'- dimethyl FAI (DMFAI), resulting in the formation of the impurity phase in perovskite thin film.[23–25] Secondly, the average size of the colloids in solution becomes larger and colloid aggregation occurs when the aging time exceeds the optimum time.[26–28] Additionally, the potential of hydrogen (pH) of solution changes from basic to acidic due to the formation of hydriodic acid (HI) during the aging process of precursor solution, which prevents the formation of α-phase of $FAPbI_3$.[29–33] Besides, I_2 is formed due to the oxidation of I^- during the aging process of the precursor solution, which causes poor performance and poor reproducibility

Z. Li, Z. Xing, X. Meng, L. Huang, X. Hu, Y. Chen
College of Chemistry and Chemical Engineering
Institute of Polymers and Energy Chemistry (IPEC)
Nanchang University
999 Xuefu Avenue, Nanchang 330031, China
E-mail: ywchen@ncu.edu.cn
H. Peng, D. Li, T. Hu
School of Physics and Materials Science
Nanchang University
999 Xuefu Avenue, Nanchang 330031, China
E-mail: huting@ncu.edu.cn
X. Meng, Y. Chen
National Engineering Research Center for Carbohydrate Synthesis/Key Lab of Fluorine and Silicon for Energy Materials and Chemistry of Ministry of Education
Jiangxi Normal University
99 Ziyang Avenue, Nanchang 330022, China
X. Hu
Peking University Yangtze Delta Institute of Optoelectronics
Nantong 226010, China
The ORCID identification number(s) for the author(s) of this article can be found under https://doi.org/10.1002/aenm.202200650.

DOI: 10.1002/aenm.202200650

 © 2022 Wiley-VCH GmbH

of the PSCs.[34] According to the above aging mechanism, the researchers have proposed various relevant stability strategies and these strategies are summarized in five main points. First of all, additives are applied to inhibit the deprotonation of MA, such as the addition of S_8,[22] triethyl borate, etc.[23] Then, reductant is applied to inhibit the oxidation of I^-, such as the addition of benzylhydrazine hydrochloride.[34] In addition, perovskite single crystal is fabricated to inhibit aging.[30] Furthermore, the optimum aging time leading to the best device efficiency and highest reproducibility is determined.[26] Lastly, the additive is applied to stabilize highly active FA^+, such as the addition of 4,4′-carbonyldiphthalic anhydride.[35] Although various strategies have been proposed to improve the stability of precursor solution, they solve the aging problem from just one aspect. And the effects of aging precursor solutions on crystal growth of efficient triple-cation mixed-halide perovskite are ignored. It is not difficult to find that the highly reactive I^- is the main culprit of the instability of precursor solution. The I^- causes the deprotonation of MA^+ to produce HI and MA, which results in a subsequent by-product and produces an impure phase in perovskite. Simultaneously, the highly reactive FA^+ is another key factor leading to the generation of by-products. Although PbI_2 has been proved to induce perovskite crystallization,[36–43] a large proportion of PbI_2 in the triple cation mixed halide PSCs will also lead to excessive I^- in the solution. As mentioned above, the stability of precursor is caused by multiple factors, typically related to reactions triggered by the A-site cation and the halogen at the X-site. So, the above reactions should be suppressed to stabilize the precursor solution.

In this work, we intend to introduce diethyl (hydroxymethyl) phosphonate (DHP) through various bonding effects, which can achieve a multi-component stabilization to improve the long-term stability of the precursor solution. The DHP could inhibit the reactivity of I^- and FA^+ to obtain a more stable precursor solution. Moreover, since the chelation interaction between the P=O of DHP and Pb^{2+}, DHP could passivate defects in perovskite to improve the film quality. In this case, the device based on a fresh DHP-doped precursor solution delivers a champion efficiency of 22.91%. The DHP-doped precursor solution is stable even after being stored at room temperature in air for 50 days and the corresponding devices maintains 81% of the initial performance.

2. Results and Discussion

Specifically, the DHP is employed as a reactive inhibitor of I^- and FA^+ (**Figure 1**a). Since the vacant orbital of the phosphorus atom in DHP with electron-withdrawing capability would interact with the lone-pair electron in I^-, the reactivity of I^- can be inhibited. In this case, the deprotonation reaction of MA^+ and the generation of I_2 and I_3^- will be suppressed. In addition, hydrogen bonds can be formed between DHP and FA^+ to further inhibit the generation of by-products. Thus, the stability of precursor solution could be improved, which will be verified. Simultaneously, due to chelation interaction of Pb^{2+} with oxygen of P=O in DHP, the DHP in the perovskite film could improve the film quality with desired stoichiometry by reducing the defects and the content of PbI_2. Figure 1b,c shows the highest occupied molecular orbit (HOMO) of MAI and the lowest unoccupied molecular orbit (LUMO) of DHP, respectively. The vacant orbital of the phosphorus atom in DHP interacts strongly with the lone-pair electron in I^-, which leads to the decrease of the electron cloud density of I^-, thus suppressing the deprotonation reaction of MA^+. For pure FAI (Figure 1d), two proton nuclear magnetic resonance (^{1}H NMR) resonance peaks corresponding to the C—H bond (≈7.8 ppm) and protons (≈8.7 ppm) of the amine groups in the FA organic part are detected, respectively. After being doped with DHP, the NMR resonance peak at ≈8.7 ppm splits into two new peaks at ≈8.6 and 8.9 ppm owing to the formation of hydrogen bonds between the N—H bond in FA^+ and the O in -OH of DHP.[35,44] Clearly, when DHP is added to PbI_2 solution, the resonance absorption peak of the DHP shifts to upfield because the strong chemical interaction between the P=O bonds of DHP and Pb^{2+} ions reduces the electron cloud density at the periphery of the H nucleus in the DHP (Figure 1e). Besides, the interaction of DHP with Pb^{2+} has also been verified by X-ray photoelectron spectroscopy (XPS) with Pb 4f XPS peaks shifting to lower binding energy (Figure S1, Supporting Information).[45]

Different solutions are prepared by dissolving mono component of the precursor in a *N*, *N*′-dimethylformamide (DMF), and dimethyl sulfoxide (DMSO) mixed solvent (4/1, v/v). As shown in Figure S2 (Supporting Information), a significant change of color is observed in the iodine-contained solutions with DHP after aging in the air for 24 h, indicating that DHP interacts strongly with the component in the iodine contained solutions. Then, ^{1}H NMR test is performed on these solutions to understand the interactions between the DHP and other mono components of the precursor. The ^{1}H NMR spectra of the MA-based and Cs-based solution (MABr, MAI, MACl, or CsI) show no new peaks and chemical shift in relation to the reaction between the MA^+ or Cs^+ and DHP (Figure S3a–d, Supporting Information). To demonstrate the strong interaction between DHP and I^-, XPS tests are utilized. Compared to pure PbI_2, the I^- binding energy changes significantly for the DHP-doped PbI_2 (Figure S4a, Supporting Information). Simultaneously, the binding energy of phosphorus in DHP is different after being added to the precursor solution (Figure S4b, Supporting Information). These phenomena prove that the phosphorus atom of DHP interacts strongly with the I^- to inhibit the reaction of I^- discussed above.

In this experiment, the addition amount of DHP in precursor solution is verified and the optimized addition amount is 2.5 mol% (Figure S5, Supporting Information). In order to prove the effect of DHP, the precursor solution with 2.5 mol% DHP with different aging time are prepared. For the solution without DHP, the ^{1}H NMR spectra (Figure 1f) of the aged sample exhibit a strong peak for the by-product MFAI and DMFAI. However, no MFAI and DMFAI are discovered in the aged precursor solution with DHP (Figure 1g). Since DHP has strong interactions with both I^- and FA^+, the deprotonation reaction of MA^+ is interrupted to avoid the formation of MFAI and DMFAI as follows.

$$MA^+ + I^- \rightarrow MA + HI \quad (1)$$

$$MA + FAI \rightarrow MFAI \quad (2)$$

© 2022 Wiley-VCH GmbH

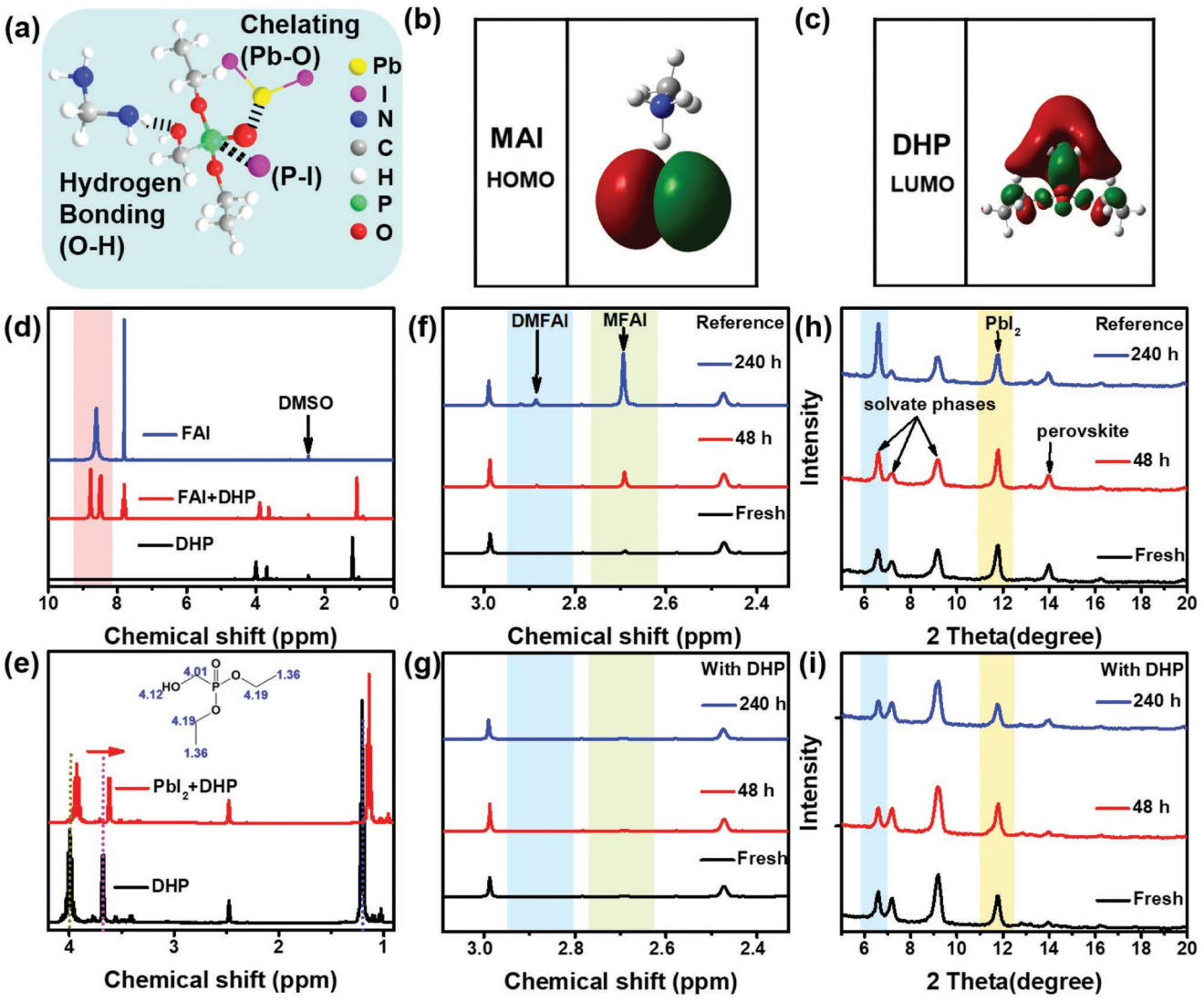

Figure 1. a) Schematic of the interaction between DHP and perovskite precursor. b) The HOMO of MAI and c) the LUMO of DHP molecule obtained with DFT calculation. Corresponding liquid-state ^{1}H NMR spectra of d) FAI, DHP and FAI with DHP, and e) PbI_2 and PbI_2 with DHP in deuterated DMSO-d_6 solution at 295 K (The inserted diagram is NMR ^{1}H estimation of DHP). The ^{1}H NMR results of perovskite /DMSO-d_6 solution f) without and g) with DHP. XRD patterns of perovskite wet films h) without and i) with DHP. (Precursor solutions aging for 48 h (red) and 240 h (blue) in air at 25 ± 5 °C with an RH of 50 ± 5%, respectively).

$$MA + MFAI \rightarrow DMFAI \quad (3)$$

It proves the DHP could improve the stability of perovskite precursor solution by inhibiting the formation of by-products. Then, for the solutions with different aging times, corresponding wet films are fabricated by spin-coating to further investigate the stability of the DHP-doped solution. Please note that anti-solvent and annealing treatment that may affect the test result is not adopted in the film fabrication, and the aging time is the aging time of precursor solution, rather than the aging time of wet film. The origin of different peaks has been marked in the XRD patterns (Figure 1h). Among them, the peaks ascribing to solvate phases of the DHP-doped sample show no difference after aging. By comparison, the peak at 6.6° ascribing to solvate phases gets stronger for the undoped sample. According to the literatures, the solvate phases are the intermediate phases of perovskite that contain DMSO and DMF, and the by-products in the aged undoped precursor solution interact with DMSO more strongly than MAI and FAI, thus leading to a stronger peak at 6.6° after aging. It proves that by-products such as MFAI and DMFAI generate in the undoped sample after aging. However, no inconspicuous change is observed for the XRD peak intensity of aged precursor solution with DHP, which demonstrates that the DHP-doped solution delivers better stability than the undoped solution (Figure 1i).

To verify whether DHP can inhibit the oxidation of I^- during the aging process, the solution is prepared by dissolving iodine contained components (FAI and CsI) in a mixed solvent with the same ratio and concentration used in the precursor solution for device fabrication. In these solutions, the absorption spectrum of PbI_2 overlaps with that of I_2 to a great extent, so PbI_2

© 2022 Wiley-VCH GmbH

is excluded in this experiment. An obvious decrement of I_2 and I_3^- is detected in UV–vis absorption spectrum of the aged solution with DHP, proving that the reactivity of I^- is well inhibited (Figure S6, Supporting Information). In addition, UV-vis absorption of the aged precursor solution with and without DHP are studied (Figure S7, Supporting Information). Because of the strong interaction between DHP and I^-, DHP-doped solution presents a significant reduction of PbI_2 and PbI_3^- by comparing with undoped precursor solution. To examine the change in colloidal size distribution after aging, dynamic light scattering (DLS) is employed (Figures S8 and S9, Supporting Information). The precursor solution with DHP processes a smaller average size and shows no difference after aging for different time, while the undoped solution presents a larger average size and colloidal aggregate with increased size after aging. For the DHP-doped precursor solution, due to the strong interaction of DHP with both I^- and FA^{2+}, further adsorption of monomers in the solution could be avoided and larger colloidal particles such as FAI-DMSO-PbI_2 are less likely to be formed. Thus, colloidal size distribution is better and does not change drastically. Finally, the stability of the solution is improved without aggregation after aging.

For the precursor solution with different aging time, the optical characterization of corresponding perovskite films are carried out to verify the anti-aging effect of DHP. It can be seen that the undoped perovskite film displays a significant decrease in intensity of the steady-state photoluminescence (PL) excited peak and UV–vis absorption spectra after aging. On the contrary, DHP-doped perovskite film displays no difference in intensity of the PL excited peak and UV–vis absorption spectra after aging (**Figure 2**a–d). To further analyze the role of DHP from the perspective of crystal structures, the XRD measurements (Figure 2e,f) are performed. With the longer aging time, the peak intensity of the (110) plane gets weaker and the peak intensity of PbI_2 gets stronger for the undoped perovskite film, indicating the perovskite film based on undoped precursor solution is not stable and suffers degradation. Alternatively, impure δ-phase $FAPbI_3$ is formed in the film when the undoped precursor solution is aging for 96 h. By comparing with the pure δ-$FAPbI_3$ (11.74°), the diffraction peak of impure

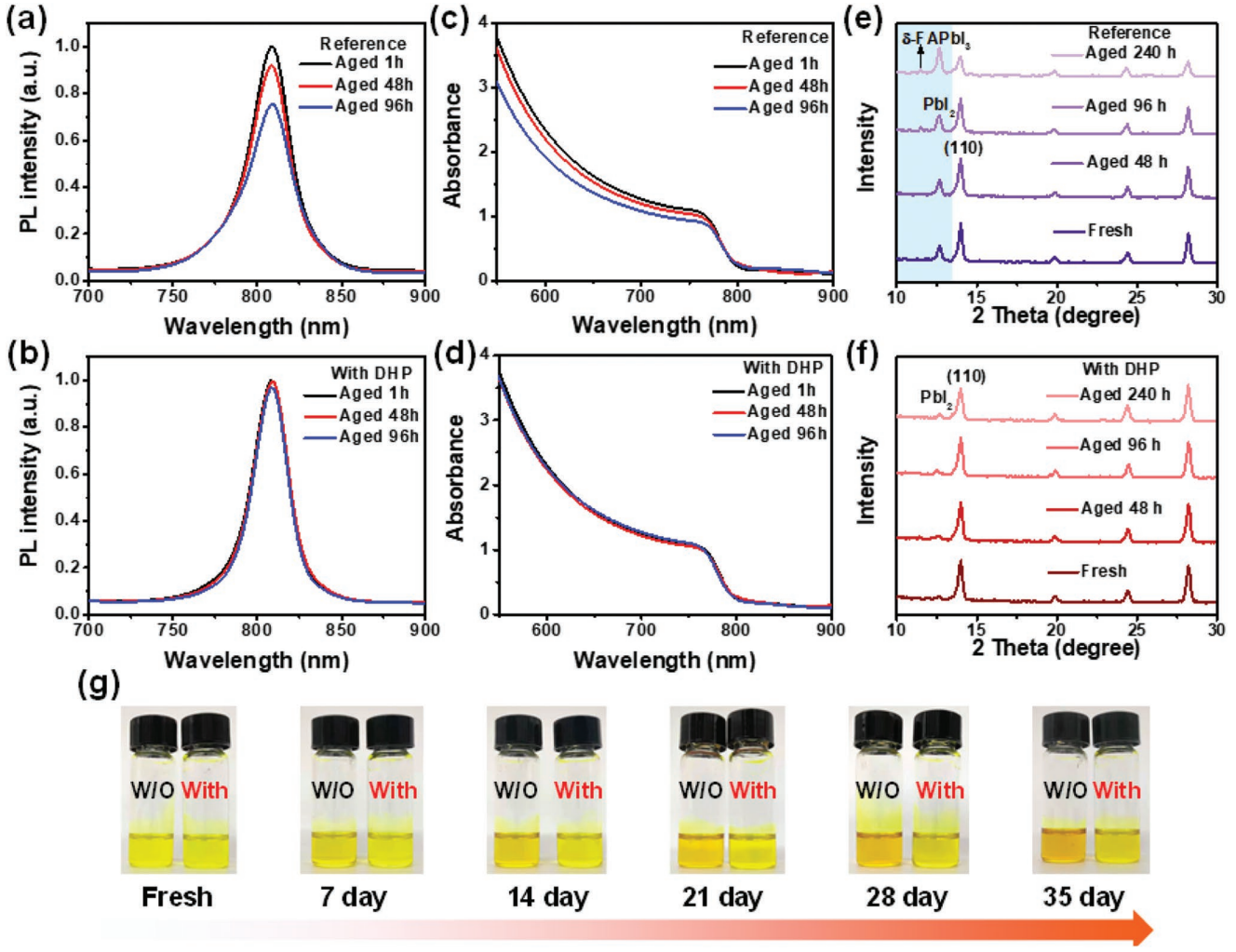

Figure 2. a,b) Steady-state PL, c,d) UV–vis absorption, and e,f) XRD patterns of perovskite films based on reference solution (a, c, and e) and solution with DHP (b,d, and f), respectively. g) Images of precursor solutions after aging in the air at 25 ± 5 °C with RH of 50 ± 5% for 35 days. The "W/O" represents the precursor solution without DHP, the "With" represents the precursor solution with DHP.

© 2022 Wiley-VCH GmbH

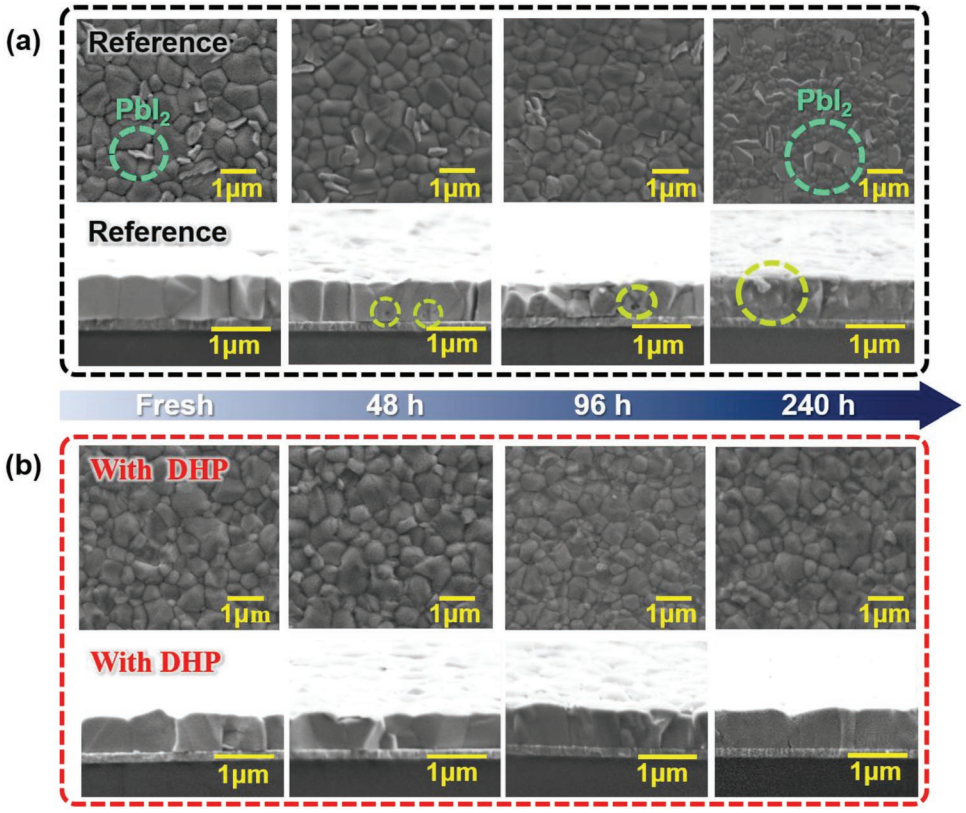

Figure 3. Top-view and cross-sectional SEM images of perovskite films based on precursor solutions a) without and b) with DHP with different aging times. (Precursor solutions aging for 48, 96, and 240 h in air at 25 ± 5 °C with RH of 50 ± 5%).

δ-phase $FAPbI_3$ (11.47°) exhibits a significant left shift because some impurities, such as MFAI and DMFAI, are included.[23] By comparison with undoped perovskite film, DHP-doped perovskite film behaves much more stable with slight change after aging and PbI_2 in the film is greatly reduced. Moreover, no peak of δ-phase $FAPbI_3$ is detected in the XRD measurement, demonstrating DHP could stabilize the precursor solution. Besides, the DHP-doped precursor solution shows no difference in color and the color of the undoped solution becomes darker after aging in the air for 35 days (Figure 2g).

Crystal quality is critical to the performance of PSCs. The standard of good film quality is large grain size, no voids, and less defect density. Good crystal quality will exhibit faster charge transfer and lower defect density, resulting in better device performance. Poor crystal quality brings about pinholes in the perovskite film, which will result in imperfect coverage of perovskite film and cause unwanted contact between the electron and hole transporting layer. As a result, the PSCs deliver a poor performance with low fill factor (FF) and open circuit voltage (V_{OC}).

To illuminate the effect of DHP on film quality, the top-view and cross-sectional scanning electron microscopy (SEM) images are present in **Figure 3**. The morphology evolution of the perovskite film based on different aging precursor solutions is investigated. As proved in the XRD result, the undoped film is not stable with a lot of PbI_2, which is also observed in the corresponding SEM images.[9,19,22] Compared to the fresh film, the cross-sectional SEM image of undoped perovskite film based on aged solution exhibit voids, and the grains are destroyed (Figure 3a). This phenomenon is caused by the by-products and reduced monomers in the aged precursor solution. On the contrary, for the DHP-doped films, no matter based on fresh precursor solution or the aged precursor solution, no obvious voids, and PbI_2 flakes are observed. Because the generation of by-products are suppressed by the DHP in the DHP-doped precursor solution (Figure 3b). This proves that DHP has a good stabilization effect on the precursor solution, which could improve the reproducibility of the perovskite film even after a long aging time.

The device performance of the corresponding PSCs is investigated by using the conventional configuration of ITO/SnO_2/perovskite/spiro-OMeTAD/Ag. Compared to the reference device with a maximum PCE of 20.6% (**Figure 4**a), the device with DHP delivers a higher PCE of 22.91% with good reproducibility (Figure 4b). Clearly, all parameters of the DHP-doped device, including V_{OC}, J_{SC}, and FF, are improved, which is due to the improved film quality with fewer defects and PbI_2. The steady-state output test provides an effective check on the operational stability of the device. A sustained and stable output efficiency can be obtained when stabilized output power for the device with DHP perovskite film is recorded under continuous AM 1.5 G, 1-sun illumination at a fixed maximum power point voltage over 300 s (Figure 4c). To quantitatively determine the trap-state density (N_t) of corresponding PSCs, electron-only devices with the configuration of ITO/SnO_2/PVK/PCBM/Ag are fabricated for comparison. The N_t is calculated with the following equation.

© 2022 Wiley-VCH GmbH

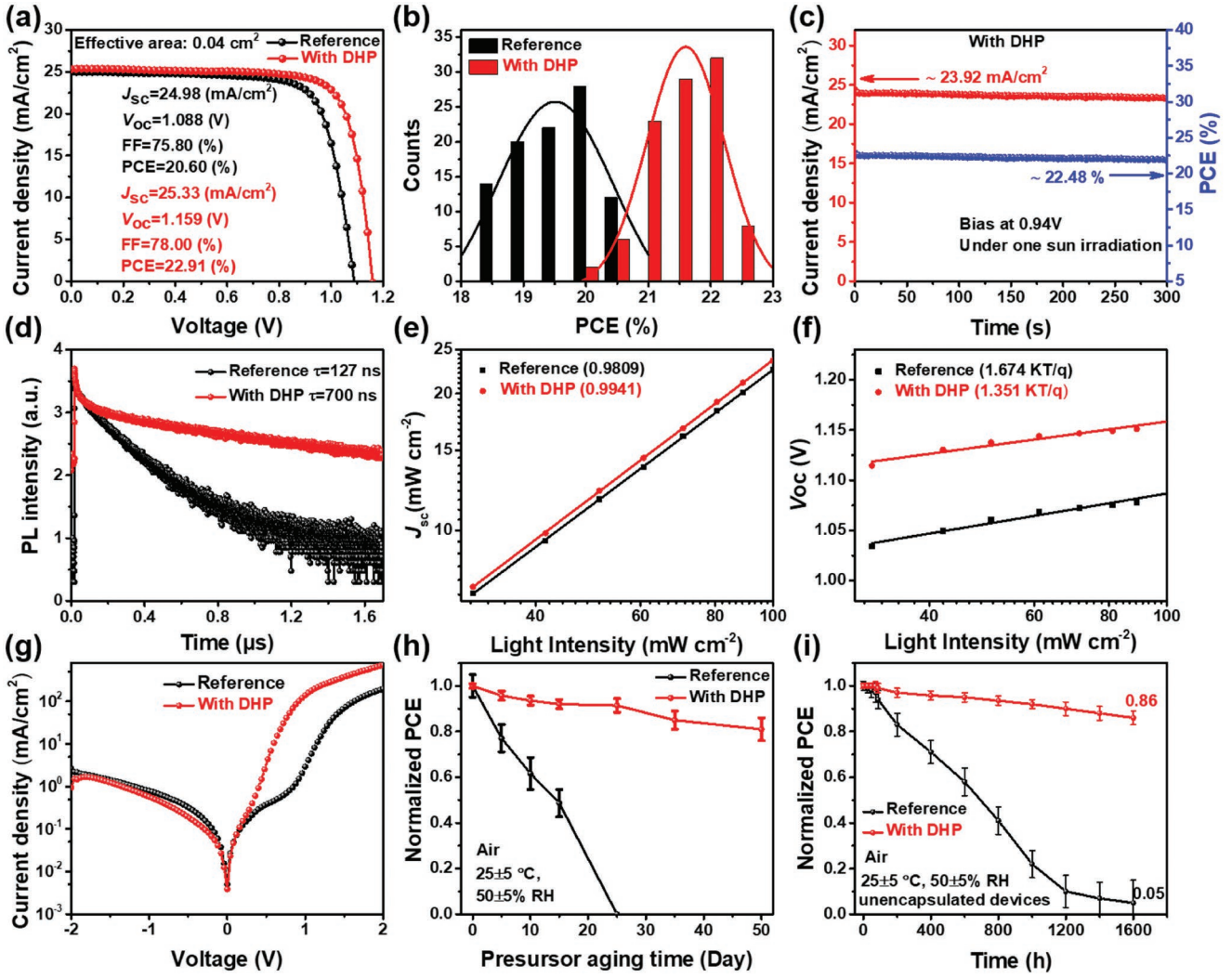

Figure 4. a) *J–V* curves and PCE data of PSCs with and without DHP. b) Reproducibility of PSCs with and without DHP. c) The steady-state photocurrent and output PCE of the PSCs with DHP at the maximum power point of 0.94 V. d) TRPL spectra of the perovskite films with and without DHP. Light intensity dependence of e) J_{SC} and f) V_{OC}. g) Dark *J--V* curves of devices with and without DHP. h) Normalization of PCE for PSCs fabricated based on different precursor solutions with different aging times. Precursor solutions are stored in air at 25 ± 5 °C. i) Long-term stability of unencapsulated devices with and without DHP by being stored in air for 1600 h with 50 ± 5% RH.

$$N_t = \frac{2\varepsilon_0\varepsilon_r V_{TFL}}{qL^2} \quad (4)$$

where ε_0 is the vacuum permittivity, q is the elemental charge, V_{TFL} is the onset voltage of the trap-filled limited region, ε_r is the relative dielectric constant, and L is the thickness of the film. From the calculation results, N_t of 9.13×10^{15} cm^{-3} for the reference devices can be obtained. In contrast, the DHP-doped devices showed a decreased N_t of 7.32×10^{15} cm^{-3} (Figure S10, Supporting Information). By comparing with that of undoped film, the N_t of DHP-doped film declined, implying the nonradiative recombination in corresponding devices is reduced. Besides, the reduction in trap-state density could also be deduced from time-resolved PL (TRPL) measurements (Figure 4d). The average carrier lifetime of reference is 127 ns, and that increases significantly to 700 ns for DHP-doped film. This demonstrates the lower trap density in the DHP-doped films, enabling less nonradiative recombination loss and prolonging lifetime. Additionally, the dependence of device current and voltage on incident light intensity is investigated. $J_{SC} \propto I^{\alpha}$, and the deviation of ideality factor $\alpha = 1$ suggests the extent of bimolecular recombination. Figure 4e indicates the reduced bimolecular recombination in the device with DHP. To judge whether trap-assisted nonradiative recombination occupies a dominant position in the device, the slope of kT/q (k: Boltzmann constant, q: elementary charge) of the plot of ΔV_{oc} versus ln(I) is employed. The slope decreases from 1.674 kT/q to 1.351 kT/q with the incorporation of DHP, which reveals a reduction in trap-assisted recombination under open-circuit conditions (Figure 4f). To verify whether the addition of DHP could suppress charge carrier recombination or not, dark-current measurements are investigated (Figure 4g). The reverse current density of the device with DHP decreased compared to that of the reference, revealing the inhibited leakage current

© 2022 Wiley-VCH GmbH

and charge carrier recombination. The external quantum efficiency (*EQE*) of the DHP-doped device is superior compared to the undoped device in the entire visible-light absorption region (Figure S11, Supporting Information), and the integrated J_{SC} of the devices well matches to the measured J_{SC} under the solar simulation. The results above confirm the effective defect passivation effect of the DHP on perovskite, which can restrain charge recombination to improve photoelectric performance.

To assess the stability of the precursor solution, precursor solutions are aging under different conditions with different time, and the corresponding devices are fabricated. First, all the precursor solutions are aging in air conditions at 25 ± 5 °C with relative humidity (RH) of 50 ± 5%. As a result, for the DHP-doped precursor solutions with an aging time of 50 days, the corresponding device retains ≈81% of its initial efficiency, but for the undoped precursor solutions with an aging time of 25 days, the PCE of the corresponding device declines to 0% (Figure 4h). Besides, the precursor solutions are also aging in N_2 conditions at 35 ± 5 °C (Figure S12, Supporting Information). The result is similar to that obtained under air condition, that DHP-doped precursor solutions is much more stable than undoped precursor solutions, which is attributed to the inhibition effect of DHP molecular on the solution.

In order to verify whether DHP could improve the device stability in addition to the device efficiency optimization, unencapsulated devices based on fresh precursor solution are fabricated and stored in air conditions at 25 ± 5 °C with 50 ± 5% RH. As shown in Figure 4i, the DHP-doped devices illustrate superior long-term stability with 86% of its original efficiency being retained after 1600 h, while the undoped devices decay seriously with only 5% of its original efficiency being retained. The DHP as a Lewis base could passivate defects such as uncoordinated lead ions, thus reducing ion migration and avoiding degradation of device performance. It is proved that the DHP could improve the stability of the precursor solution and corresponding device.

3. Conclusion

In summary, the shelf-life of the precursor solution is effectively improved by introducing DHP as a reactive inhibitor. Benefiting from the effectively inhibited reactivity of I^- and FA^+ after adding DHP, the production of by-products in the precursor is obviously suppressed. Hence, the DHP-doped precursor solution shows super stability under ambient conditions. In addition, due to chelation interaction of Pb^{2+} with oxygen of P=O in DHP, the DHP in the perovskite film could improve the film quality with desired stoichiometry by reducing the defects and the content of PbI_2. Due to the multiple chemical bonding, the efficient PSCs are obtained with excellent performance reproducibility. This strategy offers a direction to the commercial feasibility of PSCs based on excellent stable precursor solutions.

Supporting Information

Supporting Information is available from the Wiley Online Library or from the author.

Acknowledgements

Y.C., T.H., and X.H. thank the support from the National Natural Science Foundation of China (NSFC) (52163019, 22005131, 52173169, and U20A20128). T.H. and X.M. thank the support from the China Postdoctoral Science Foundation (2021M700060, 2021M691394). T.H. thanks the support from the Postdoctoral Science Foundation of Jiangxi Province (2020KY11) and the Natural Science Foundation of Jiangxi Province (20202BAB212002).

Conflict of Interest

The authors declare no conflict of interest.

Author Contributions

Z.L. and Z.X. contributed equally to this work. Y.C., T.H. conceived and designed the experiments. Z.L., Z.X. fabricated the PSCs devices. L.H., H.P., and D.L. characterized and analyzed the device performance and morphology of PSCs. Z.X., X.H., and Z.L. characterized and analyzed the various photoelectric properties. Z.L., Z.X., and T.H. completed the writing of the manuscript.

Data Availability Statement

Research data are not shared.

Keywords

crystal growth, reactive inhibition, reproducibility, solution stability, triple-cation perovskites

Received: February 23, 2022
Revised: May 6, 2022
Published online:

[1] S. Ning, A. Kumar, K. Klyukin, E. Cho, J. H. Kim, T. Su, H. S. Kim, J. M. LeBeau, B. Yildiz, C. A. Ross, *Nat. Commun.* **2021**, *12*, 4298.
[2] H. J. Eggimann, J. B. Patel, M. B. Johnston, L. M. Herz, *Nat. Commun.* **2020**, *11*, 5525.
[3] Q. Dong, C. Zhu, M. Chen, C. Jiang, J. Guo, Y. Feng, Z. Dai, S. K. Yadavalli, M. Hu, X. Cao, Y. Li, Y. Huang, Z. Liu, Y. Shi, L. Wang, N. P. Padture, Y. Zhou, *Nat. Commun.* **2021**, *12*, 973.
[4] S. Reichert, Q. An, Y.-W. Woo, A. Walsh, Y. Vaynzof, C. Deibel, *Nat. Commun.* **2020**, *11*, 6098.
[5] G. E. Eperon, S. D. Stranks, C. Menelaou, M. B. Johnston, L. M. Herz, H. J. Snaith, *Energy Environ. Sci.* **2014**, *7*, 982.
[6] H. Min, D. Y. Lee, J. Kim, G. Kim, K. S. Lee, J. Kim, M. J. Paik, Y. K. Kim, K. S. Kim, M. G. Kim, T. J. Shin, S. SeokIl, *Nature* **2021**, *598*, 444.
[7] D. Li, Z. Xing, L. Huang, X. Meng, X. Hu, T. Hu, Y. Chen, *Adv. Mater.* **2021**, *33*, 2101823.
[8] T. M. Brenner, D. A. Egger, L. Kronik, G. Hodes, D. Cahen, *Nat. Rev. Mater.* **2016**, *1*, 15007.
[9] S. A. More, R. Halor, S. Raees, S. S. Ghosh, *J. Mater. Sci. Mater. Electron.* **2020**, *31*, 17995.
[10] W. Nie, H. Tsai, R. Asadpour, A. J. Neukirch, G. Gupta, J. J. Crochet, M. Chhowalla, S. Tretiak, M. A. Alam, H. Wang, *Science* **2015**, *347*, 522.

© 2022 Wiley-VCH GmbH

[11] Y. Rong, Z. Tang, Y. Zhao, X. Zhong, S. Venkatesan, H. Graham, M. Patton, Y. Jing, A. M. Guloy, Y. Yao, *Nanoscale* **2015**, *7*, 10595.
[12] M. I. Saidaminov, A. L. Abdelhady, B. Murali, E. Alarousu, V. M. Burlakov, W. Peng, I. Dursun, L. Wang, Y. He, G. Maculan, A. Goriely, T. Wu, O. F. Mohammed, O. M. Bakr, *Nat. Commun.* **2015**, *6*, 7586.
[13] X. Gong, M. Li, X. B. Shi, H. Ma, Z. K. Wang, L. S. Liao, *Adv. Funct. Mater.* **2015**, *25*, 6671.
[14] C. G. Wu, C. H. Chiang, Z. L. Tseng, M. K. Nazeeruddin, A. Hagfeldt, M. Grätzel, *Energy Environ. Sci.* **2015**, *8*, 2725.
[15] Z. Wang, D. P. McMeekin, N. Sakai, S. van Reenen, K. Wojciechowski, J. B. Patel, M. B. Johnston, H. J. Snaith, *Adv. Mater.* **2017**, *29*, 1604186
[16] J. Pan, C. Mu, Q. Li, W. Li, D. Ma, D. Xu, *Adv. Mater.* **2016**, *28*, 8309.
[17] K. G. Stamplecoskie, J. S. Manser, P. V. Kamat, *Energy Environ. Sci.* **2015**, *8*, 208.
[18] Y. Guo, K. Shoyama, W. Sato, E. Nakamura, *Adv. Energy Mater.* **2016**, *6*, 1502317.
[19] Q. Chen, H. Zhou, T. Bin Song, S. Luo, Z. Hong, H. S. Duan, L. Dou, Y. Liu, Y. Yang, *Nano Lett.* **2014**, *14*, 4158.
[20] A. Younis, C. H. Lin, X. Guan, S. Shahrokhi, C. Y. Huang, Y. Wang, T. He, S. Singh, L. Hu, J. R. D. Retamal, J. H. He, T. Wu, *Adv. Mater.* **2021**, *33*, 2005000
[21] Y. Zhang, Z. Zhou, F. Ji, Z. Li, G. Cui, P. Gao, E. Oveisi, M. K. Nazeeruddin, S. Pang, *Adv. Mater.* **2018**, *30*, 1707143.
[22] H. Min, G. Kim, M. J. Paik, S. Lee, W. S. Yang, M. Jung, S. SeokIl, *Adv. Energy Mater.* **2019**, *9*, 1803476.
[23] X. Wang, Y. Fan, L. Wang, C. Chen, Z. Li, R. Liu, H. Meng, Z. Shao, X. Du, H. Zhang, G. Cui, S. Pang, *Chem* **2020**, *6*, 1369.
[24] C. Grundmann, A. Kreutzberger, *J. Am. Chem. Soc.* **1955**, *77*, 6559.
[25] O. Chemie, *Chem.Ber* **1965**, *493*, 2887.
[26] P. Boonmongkolras, D. Kim, E. M. Alhabshi, I. Gereige, B. Shin, *RSC Adv.* **2018**, *8*, 21551.
[27] D. P. McMeekin, Z. Wang, W. Rehman, F. Pulvirenti, J. B. Patel, N. K. Noel, M. B. Johnston, S. R. Marder, L. M. Herz, H. J. Snaith, *Adv. Mater.* **2017**, *29*, 1607039.
[28] C. Ran, W. Gao, N. Li, Y. Xia, Q. Li, Z. Wu, H. Zhou, Y. Chen, M. Wang, W. Huang, *ACS Energy Lett.* **2019**, *4*, 358.
[29] Y. H. Park, I. Jeong, S. Bae, H. J. Son, P. Lee, J. Lee, C.-H. Lee, M. J. Ko, *Adv. Funct. Mater.* **2017**, *27*, 1605988.
[30] G. S. Shin, Y. Zhang, N.-G. Park, *ACS Appl. Mater. Interfaces* **2020**, *12*, 15167.
[31] M. Qin, J. Cao, T. Zhang, J. Mai, T.-K. Lau, S. Zhou, Y. Zhou, J. Wang, Y.-J. Hsu, N. Zhao, J. Xu, X. Zhan, X. Lu, *Adv. Energy Mater.* **2018**, *8*, 1703399.
[32] Y. Zhou, J. Kwun, H. F. Garces, S. Pang, N. P. Padture, *Chem. Commun.* **2016**, *52*, 7273.
[33] J.-W. Lee, D.-H. Kim, H.-S. Kim, S.-W. Seo, S. M. Cho, N.-G. Park, *Adv. Energy Mater.* **2015**, *5*, 1501310.
[34] S. Chen, X. Xiao, H. Gu, J. Huang, *Sci. Adv.* **2021**, *7*, eabe8130.
[35] J. Zhu, D. H. Kim, J. D. Kim, D. G. Lee, W. Bin Kim, S. W. Chen, J. Y. Kim, J. M. Lee, H. Lee, G. S. Han, T. K. Ahn, H. S. Jung, *ACS Energy Lett.* **2021**, *6*, 3425.
[36] M. U. Rothmann, J. S. Kim, J. Borchert, K. B. Lohmann, C. M. O'Leary, A. A. Sheader, L. Clark, H. J. Snaith, M. B. Johnston, P. D. Nellist, L. M. Herz, *Science* **2020**, *370*, eabb5940.
[37] S. H. Cho, J. Byeon, K. Jeong, J. Hwang, H. Lee, J. Jang, J. Lee, T. Kim, K. Kim, M. Choi, Y. S. Lee, *Adv. Energy Mater.* **2021**, *11*, 2100555.
[38] B. Li, D. Binks, G. Cao, J. Tian, *Small* **2019**, *15*, 1903613.
[39] B. Dou, L. M. Wheeler, J. A. Christians, D. T. Moore, S. P. Harvey, J. J. Berry, F. S. Barnes, S. E. Shaheen, M. F. A. M. van Hest, *ACS Energy Lett.* **2018**, *3*, 979.
[40] Q. Jiang, Y. Zhao, X. Zhang, X. Yang, Y. Chen, Z. Chu, Q. Ye, X. Li, Z. Yin, J. You, *Nat. Photonics* **2019**, *13*, 460.
[41] G. S. Shin, S. Kim, Y. Zhang, N. Park, *Small Methods* **2020**, *4*, 1900398.
[42] M. Kim, G.-H. Kim, T. K. Lee, I. W. Choi, H. W. Choi, Y. Jo, Y. J. Yoon, J. W. Kim, J. Lee, D. Huh, H. Lee, S. K. Kwak, J. Y. Kim, D. S. Kim, *Joule* **2019**, *3*, 2179.
[43] J. C. Hamill, J. C. Sorli, I. Pelczer, J. Schwartz, Y.-L. Loo, *Chem. Mater.* **2019**, *31*, 2114.
[44] A. Krishna, A. Hagfeldt, Z. Zhou, T. Gallet, M. Dankl, O. Ouellette, F. Eickemeyer, H. Zhang, M. Mensi, S. M. Zakeeruddin, U. Roethlisberger, G. N. M. Reddy, A. Redinger, M. Graetzel, F. Fu, in *Proc. 13th Conf. Hybrid Org. Photovoltaics*, Fundació Scito, València, **2021**.
[45] L. Xu, J. Li, B. Cai, J. Song, F. Zhang, T. Fang, H. Zeng, *Nat. Commun.* **2020**, *11*, 3902.

© 2022 Wiley-VCH GmbH